Cylindrical-water-resonator-based ultrabroadband microwave absorber

REN, Jian; YIN, Jia Yuan

Published in:
Optical Materials Express

Published: 01/08/2018

Document Version:
Final Published version, also known as Publisher's PDF, Publisher's Final version or Version of Record

Published version (DOI):
10.1364/OME.8.002060

Publication details:
REN, J., & YIN, J. Y. (2018). Cylindrical-water-resonator-based ultrabroadband microwave absorber. *Optical Materials Express*, *8*(8), 2060-2071. https://doi.org/10.1364/OME.8.002060

Research Article | Vol. 8, No. 8 | 1 Aug 2018 | OPTICAL MATERIALS EXPRESS 2060
Optical Materials EXPRESS

Cylindrical-water-resonator-based ultra-broadband microwave absorber

JIAN REN[1,3] AND JIA YUAN YIN[2,3,*]

[1]*The State Key Laboratory of Millimeter Waves and Department of Electronic Engineering, City University of Hong Kong, Kowloon, 000000 Hong Kong SAR, China*
[2]*School of Physics and Optoelectronic Engineering, Xidian University, Xi'an, 710071 Shaanxi, China*
[3]*These authors contributed equally to this work*
**email: jyyin@xidian.edu.cn*

Abstract: In this study, a cylindrical-water-resonator-based absorber with an ultra-broad operating band at microwave wavelengths is demonstrated theoretically and experimentally. By utilizing the dielectric resonator mode, spoof surface plasmon polariton mode, and grating mode of the cylindrical water resonator, the proposed absorber exhibits an absorptivity higher than 90% over almost the entire ultra-broad operating band from 5.58 to 24.21 GHz, with a relative bandwidth as high as 125%. The angular tolerance and thermal stability of the proposed absorber are simulated, and the results indicate that the absorber performs well in a wide range of angles of incidence and exhibits a weak dependence on the water temperature. The low cost, ultra-broad operating band, good wide-angle characteristics, and thermal stability make the absorber promising for applications in antenna measurement, stealth technology, and energy harvesting.

OCIS codes: (050.6624) Subwavelength structures; (350.4010) Microwaves; (350.2450) Filters, absorption.

References and links

1. C. R. Paul, *Introduction to Electromagnetic Compatibility* (John Wiley & Sons, 2006).
2. G. Li, X. Chen, O. Li, C. Shao, Y. Jiang, L. Huang, B. Ni, W. Hu, and W. Lu, "A novel plasmonic resonance sensor based on an infrared perfect absorber," J. Phys. D Appl. Phys. **45**(20), 205102 (2012).
3. J. Grant, I. Escorcia-Carranza, C. Li, I. J. McCrindle, J. Gough, and D. R. Cumming, "A monolithic resonant terahertz sensor element comprising a metamaterial absorber and micro-bolometer," Laser Photonics Rev. **7**(6), 1043–1048 (2013).
4. P. D. Mauskopf, J. J. Bock, H. Del Castillo, W. L. Holzapfel, and A. E. Lange, "Composite infrared bolometers with Si_3N_4 micromesh absorbers," Appl. Opt. **36**(4), 765–771 (1997).
5. J. M. Gildemeister, A. T. Lee, and P. L. Richards, "Monolithic arrays of absorber-coupled voltage-biased superconducting bolometers," Appl. Phys. Lett. **77**(24), 4040–4042 (2000).
6. M. Bagmanci, M. Karaaslan, E. Unal, O. Akgol and C. Sabah, "Extremely-broad band metamaterial absorber for solar energy harvesting based on star shaped resonator," Opt. Quant. Electron. **49**(7), 257 (2017).
7. P. Li, B. Liu, Y. Ni, K. K. Liew, J. Sze, S. Chen, and S. Shen, "Large-scale nanophotonic solar selective absorbers for high-efficiency solar thermal energy conversion," Adv. Mater. **27**(31), 4585–4591 (2015).
8. H. Wang, Y. Yang, and L. P. Wang, "Switchable wavelength-selective and diffuse metamaterial absorber/emitter with a phase transition spacer layer," Appl. Phys. Lett. **105**(7), 071907 (2014).
9. M. Diem, T. Koschny, and C. M. Soukoulis, "Wide-angle perfect absorber/thermal emitter in the terahertz regime," Phys. Rev. B **79**(3), 033101 (2009).
10. Y. Matsuno and A. Sakurai, "Perfect infrared absorber and emitter based on a large-area metasurface," Opt. Mater. Express **7**(2), 618–626 (2017).
11. B. A. Munk, *Frequency Selective Surfaces: Theory and Design* (Wiley Online Library, 2000).
12. E. F. Knott, J. Shaeffer, and M. Tuley, *Radar Cross Section* (SciTech Publishing, 2004).
13. A. Ansari and M. J. Akhtar, "Co/graphite based light weight microwave absorber for electromagnetic shielding and stealth applications," Mater. Res. Express **4**, 1 (2017).
14. A. P. Raman, M. A. Anoma, L. Zhu, E. Rephaeli, and S. Fan, "Passive radiative cooling below ambient air temperature under direct sunlight," Nature **515**(7528), 540–544 (2014).
15. T. Liu and J. Takahara, "Ultrabroadband absorber based on single-sized embedded metal-dielectric-metal structures and application of radiative cooling," Opt. Express **25**(12), A612–A627 (2017).
16. D. Wu, C. Liu, Z. H. Xua, Y. M. Liu, Z. Y. Yu, L. Yu, L. Chen, R. F. Li, R. Ma, and H. Ye, "The design of ultra-broadband selective near-perfect absorber based on photonic structures to achieve near-ideal daytime radiative cooling," Mater. Des. **139**, 104–111 (2018).

#330952 https://doi.org/10.1364/OME.8.002060
Journal © 2018 Received 9 May 2018; revised 21 Jun 2018; accepted 24 Jun 2018; published 2 Jul 2018

Optical Materials EXPRESS

17. H. Severin, "Nonreflecting absorbers for microwave radiation," IRE Trans. Antennas Propag. **4**(3), 385–392 (1956).
18. N. I. Landy, S. Sajuyigbe, J. J. Mock, D. R. Smith, and W. J. Padilla, "Perfect metamaterial absorber," Phys. Rev. Lett. **100**(20), 207402 (2008).
19. J. Kim, K. Han, and J. W. Hahn, "Selective dual-band metamaterial perfect absorber for infrared stealth technology," Sci. Rep. **7**(1), 6740 (2017).
20. G. Yao, F. Ling, J. Yue, C. Luo, J. Ji, and J. Yao, "Dual-band tunable perfect metamaterial absorber in the THz range," Opt. Express **24**(2), 1518–1527 (2016).
21. X. Y. Peng, B. Wang, S. Lai, D. H. Zhang, and J. H. Teng, "Ultrathin multi-band planar metamaterial absorber based on standing wave resonances," Opt. Express **20**(25), 27756–27765 (2012).
22. G. D. Wang, M. H. Liu, X. W. Hu, L. H. Kong, L. L. Cheng and Z. Q. Chen, "Multi-band microwave metamaterial absorber based on coplanar Jerusalem crosses," Chinese Phys. B **23**, 1 (2014).
23. L. La Spada and L. Vegni, "Metamaterial-based wideband electromagnetic wave absorber," Opt. Express **24**(6), 5763–5772 (2016).
24. S. J. Li, J. Gao, X. Y. Cao, Z. Zhang, T. Liu, Y. J. Zheng, C. Zhang, and G. Zheng, "Hybrid metamaterial device with wideband absorption and multiband transmission based on spoof surface plasmon polaritons and perfect absorber," Appl. Phys. Lett. **106**(18), 181103 (2015).
25. C. Hu, X. Li, Q. Feng, X. Chen, and X. Luo, "Investigation on the role of the dielectric loss in metamaterial absorber," Opt. Express **18**(7), 6598–6603 (2010).
26. R. Yahiaoui, H. Němec, P. Kužel, F. Kadlec, C. Kadlec, and P. Mounaix, "Broadband dielectric terahertz metamaterials with negative permeability," Opt. Lett. **34**(22), 3541–3543 (2009).
27. R. Kakimi, M. Fujita, M. Nagai, M. Ashida, and T. Nagatsuma, "Capture of a terahertz wave in a photonic-crystal slab," Nat. Photonics **8**(8), 657–663 (2014).
28. S. Yin, J. Zhu, W. Xu, W. Jiang, J. Yuan, G. Yin, L. Xie, Y. Ying, and Y. Ma, "High-performance terahertz wave absorbers made of silicon-based metamaterials," Appl. Phys. Lett. **107**(7), 073903 (2015).
29. C. Hua and Z. Shen, "Shunt-excited sea-water monopole antenna of high efficiency," IEEE Trans. Antenn. Propag. **63**(11), 5185–5190 (2015).
30. M. Zou, Z. Shen, and J. Pan, "Frequency-reconfigurable water antenna of circular polarization," Appl. Phys. Lett. **108**(1), 014102 (2016).
31. Y. Li and K.-M. Luk, "A water dense dielectric patch antenna," IEEE Access **3**, 274–280 (2015).
32. J. Sun and K.-M. Luk, "A wideband low cost and optically transparent water patch antenna with omnidirectional conical beam radiation patterns," IEEE Trans. Antenn. Propag. **65**(9), 4478–4485 (2017).
33. Z. Shen, H. Yang, X. Huang, and Z. Yu, "Design of negative refractive index metamaterial with water droplets using 3D-printing," J. Opt. **19**(11), 115101 (2017).
34. A. Andryieuski, S. M. Kuznetsova, S. V. Zhukovsky, Y. S. Kivshar, and A. V. Lavrinenko, "Water: Promising opportunities for tunable all-dielectric electromagnetic metamaterials," Sci. Rep. **5**(1), 13535 (2015).
35. I. V. Stenishchev and A. A. Basharin, "Toroidal response in all-dielectric metamaterials based on water," Sci. Rep. **7**(1), 9468 (2017).
36. X. Cai, S. Zhao, M. Hu, J. Xiao, N. Zhang, and J. Yang, "Water based fluidic radio frequency metamaterials," J. Appl. Phys. **122**(18), 184101 (2017).
37. M. Odit, P. Kapitanova, A. Andryieuski, P. Belov, and A. V. Lavrinenko, "Experimental demonstration of water based tunable metasurface," Appl. Phys. Lett. **109**(1), 011901 (2016).
38. R. E. Jacobsen, A. V. Lavrinenko, and S. Arslanagic, "Water-based metasurfaces for effective switching of microwaves," IEEE Antennas Wirel. Propag. Lett. **17**(4), 571–574 (2018).
39. Y. J. Yoo, S. Ju, S. Y. Park, Y. Ju Kim, J. Bong, T. Lim, K. W. Kim, J. Y. Rhee, and Y. Lee, "Metamaterial absorber for electromagnetic waves in periodic water droplets," Sci. Rep. **5**(1), 14018 (2015).
40. W. Zhu, I. D. Rukhlenko, F. Xiao, C. He, J. Geng, X. Liang, M. Premaratne, and R. Jin, "Multiband coherent perfect absorption in a water-based metasurface," Opt. Express **25**(14), 15737–15745 (2017).
41. H. Xiaojun, Y. Helin, S. Zhaoyang, C. Jiao, L. Hail, and Y. Zetai, "Water-injected all-dielectric ultra-wideband and prominent oblique incidence metamaterial absorber in microwave regime," J. Phys. D Appl. Phys. **50**(38), 385304 (2017).
42. Y. Pang, J. Wang, Q. Cheng, S. Xia, X. Y. Zhou, Z. Xu, T. J. Cui, and S. Qu, "Thermally tunable water-substrate broadband metamaterial absorbers," Appl. Phys. Lett. **110**(10), 104103 (2017).
43. Q. Song, W. Zhang, P. C. Wu, W. Zhu, Z. X. Shen, P. H. J. Chong, Q. X. Liang, Z. C. Yang, Y. L. Hao and H. Cai, "Water-resonator-based metasurface: An ultrabroadband and near-Unity absorption," Adv. Opt. Mater. **5**, 8 (2017).
44. D. J. Gogoi and N. S. Bhattacharyya, "Embedded dielectric water "atom" array for broadband microwave absorber based on Mie resonance," J. Appl. Phys. **122**(17), 175106 (2017).
45. J. Xie, W. Zhu, I. D. Rukhlenko, F. Xiao, C. He, J. Geng, X. Liang, R. Jin, and M. Premaratne, "Water metamaterial for ultra-broadband and wide-angle absorption," Opt. Express **26**(4), 5052–5059 (2018).
46. J. Zhao, S. Wei, C. Wang, K. Chen, B. Zhu, T. Jiang, and Y. Feng, "Broadband microwave absorption utilizing water-based metamaterial structures," Opt. Express **26**(7), 8522–8531 (2018).
47. W. Ellison, "Permittivity of pure water at standard atmospheric pressure, over the frequency range 0–25 THz and the temperature range 0–100 °C," J. Phys. Chem. Ref. Data **36**(1), 1–18 (2007).

Optical Materials EXPRESS

48. Y. Pang, Y. Shen, Y. Li, J. Wang, Z. Xu, and S. Qu, "Water-based metamaterial absorbers for optical transparency and broadband microwave absorption," J. Appl. Phys. **123**(15), 155106 (2018).
49. G. S. Kell, Density, "Thermal expansivity, and compressibility of liquid water from 0° to 150°: Correlations and tables for atmospheric pressure and saturation reviewed and expressed on 1968 temperature scale," J. Chem. Eng. Data **20**(1), 97–105 (1975).

1. Introduction

For a long time, electromagnetic (EM) absorbers have attracted significant attention for their wide use and potential applications in EM compatibility [1], sensors [2,3], bolometers [4,5], solar energy harvesting [6,7], thermal emitters [8–10], stealth technology [11–13], and emerging passive cooling technologies [14–16]. In this context, numerous methods have been investigated to obtain flexible control of the different features of EM absorbers, such as the working frequency, absorptivity, and polarization response. Among these features, the operating bandwidth is one of the most pressing issues as wide-bandwidth absorbers are highly desired in different applications. To obtain wider operating bandwidths, multilayer structures [11] and lossy materials with a tapered shape [17] are commonly used, which may result in a bulk volume and high cost. In 2008, a perfect metamaterial absorber (PMA) was first proposed by Landy *et al.* [18], providing the possibility to design absorbers with an extremely low thickness. After that, many attempts have focused on metamaterial/metasurface-based absorbers from the microwave band to optical band. Limited by the resonance property, the operating bandwidth of the PMA is usually narrow. To address this issue, PMAs with dual- [19,20] and multi- [21,22] operating bands have been investigated during the past decade and the combination of these multi-operating bands has helped the broadband property to be obtained [23,24]. In addition, it has been proved that the absorption in PMAs is mainly caused by dielectric loss [25,26], implying that the use of high-dielectric-loss materials has a large potential in the design of near-unity absorbers with wide operating bands [27,28].

Water, as one of the most accessible materials in nature, has been widely investigated in EM areas because of its advantages of low cost, low environmental pollution, and easy accessibility. It has been widely used in the design of different microwave antennas such as monopole antennas [29], reconfigurable antennas [30], and dielectric patch antennas [31,32]. Recently, water has also become a hotspot in the design of all-dielectric metamaterials [33–35], which can support electric and/or magnetic resonance through the appropriate tuning of the shape or orientation of dielectric resonators (DRs). Further, because of the fluidity of water, it is easy to realize tunable all-dielectric metamaterials [36,37]. Most recently, the water-based metasurface utilizing "rod-like" water resonator has also been investigated for effective switching of microwaves and the switching can be tuned mechanically by rotating the metasurface [38].

Unlike other microwave dielectrics, the imaginary part of the permittivity of water, ε'', is quite large in the microwave band, making it exhibit a high dielectric loss, suitable for the design of an EM absorber with high absorptivity. At the same time, the real part of the permittivity, ε', depends strongly on frequency, making it possible to obtain water-based microwave components with an ultra-broad operating bandwidth. However, one issue that limits the direct use of water as a microwave absorber is the impedance mismatch at the interface of water and air, which will prevent EM waves from propagating into the water, leading to a low absorption. In this context, plenty of previous studies have been carried out to eliminate such mismatch. Taking advantage of the high dielectric loss of water, different water-based wideband EM absorbers have been proposed during the past few years. In 2015, Yoo *et al.* proposed a metamaterial absorber using periodic water droplets for the first time, covering the range of 8–18 GHz [39]. Grid-shaped water-based metasurfaces were also designed in [40] and [41] for multiband-coherent-effect absorption and ultra-wideband absorption, respectively. Pang *et al.* proposed a thermally tunable broadband metamaterial absorber based on a water substrate [42]. In [43], a water resonator with a spherical cap shape

Optical Materials EXPRESS

is presented for wide microwave absorption and dynamically tunable absorption by changing the height of the water resonator. Rectangular water resonators with a relative bandwidth of 28.8% have also been investigated [44]. In [45], a water-based metamaterial absorber was designed by introducing a cylindrical hole into a water plate. This kind of absorber exhibited an ultra-broadband operating frequency of 12–29.6 GHz. Besides, the water cube has also been studied for broadband microwave absorbers [46].

In this paper, a cylindrical-water-resonator-based absorber for microwave absorption is proposed. Both the DR mode, spoof surface plasmon polariton (SPP) mode and grating mode of the cylindrical water resonator are excited, resulting in near-unity absorption over an ultra-broad bandwidth. Unlike previously designed absorbers based on a spherical water resonator or water plate, our cylindrical water resonator is investigated. Taking advantage of the frequency-dependent permittivity of water in the band of interest, the water resonator can resonate in its DR mode over a wide band at a lower frequency with two absorption peaks, whereas at higher frequencies, the spoof SPP mode and grating mode of the water resonator can be excited over a wide band with two more absorption peaks. Through the optimization of the dimensions of the water resonator, an ultra-broad absorption band can be achieved over the range from 5.58 to 24.21 GHz, with an absorptivity higher than 90%. The relative bandwidth reaches as high as 125%. Numerical simulations and experiments are carried out to verify the working principle of the designed ultra-broadband absorber. The good agreement between the simulated and measured results implies the validity of the proposed design. The angular tolerance of the absorber is also discussed, showing the high absorptivity under wide angles of incidence. Finally, the absorptivity under different temperatures is investigated to evaluate the performance of the proposed absorber. The good performance indicates that the designed absorber is promising for different applications, such as radar cross-section reduction, low-cost anechoic chambers, and stealth technology.

2. Design of a cylindrical-water-resonator-based absorber

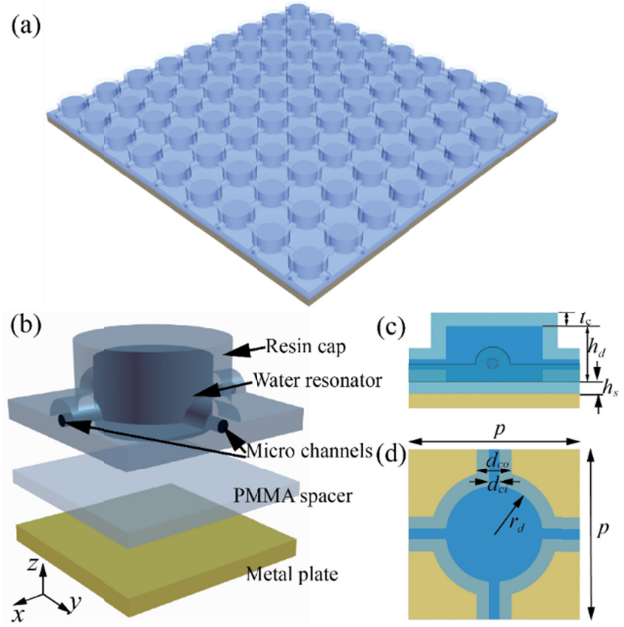

Fig. 1. (a) Schematic of the cylindrical-water-resonator-based ultra-broadband absorber. (b) Exploded view of the unit cell of the absorber. Each part of the unit cell is arranged layer-by-layer. (c) Side view and (d) top view of the unit cell. The geometrical parameters are as follows: p = 11.4 mm, r_d = 3.2 mm, h_d = 3.8 mm, t_c = 1 mm, h_s = 0.8 mm, d_{ci} = 0.6 mm, and d_{co} = 2.2 mm.

Optical Materials EXPRESS

The cylindrical-water-resonator-based absorber is illustrated in Fig. 1(a), and Fig. 1(b) describes each single element. Figures 1(c) and (d) show the side view and top view of the unit cell of the absorber, respectively, and the dimensions of the unit cell are marked in the figures. The unit cell is periodically extended in the x and y-directions with a lattice period of p. Each cell of the absorber consists of a water cylinder placed between a cylindrical resin cap and a bottom spacer layer made of polymethyl methacrylate (PMMA). The water cylinder has a radius of r_d and height of h_d, while the height of the PMMA spacer is denoted as h_s. A metallic layer, copper, is bonded to the backside of the PMMA spacer as the backplate of the whole element. The resin cylindrical cap and bottom spacer layer form the container of the water resonator. In order to inject water into the container, two microchannels are added in the resin cap, with a diameter of d_{ci} = 0.6 mm. As the size of the microchannels is much smaller than the operating wavelength, their effect can be neglected. The dimensions of the absorber are optimized using the genetic algorithm integrated in CST Microwave Studio software to obtain the wide operating band. At the same time, as the absorbers are widely used in military and communication applications, we have set the operating band to cover the whole X-band (8–12 GHz) and Ku-band (12–18 GHz). By optimizing, good impedance matching between the air and absorber can be obtained and near-unity absorption appears over the broadband because of the high dielectric loss of water.

3. Numerical analysis and measured results

In order to investigate the working principle of the proposed absorber and optimize the design, numerical analysis is first carried out. The commercial full-wave simulation software CST Microwave Studio based on the finite integration technique is used for the numerical simulation. In the simulation, the unit cell boundary is used, and the incident EM wave is assumed to propagate from the + z axis. Because of the symmetry of the structure, the absorber is independent of the polarization of the incident wave, and the x-polarized wave is assumed. For metal-backed absorbers, the absorptivity in the simulation can be defined as $A(\omega) = 1 - R(\omega)$, where $R(\omega)$ represents the reflectivity and can be calculated through the simulated S-parameters.

The dielectric constants of the resin and PMMA for the container of the water resonators are set as $\varepsilon_r = 3 \times (1 - j0.01)$ and $\varepsilon_r = 2.55 \times (1 - j0.001)$, respectively. To represent the microwave dielectric characteristic of pure water, the Debye model is used in the numerical simulation. Figure 2 shows the dielectric constant of pure water at ambient temperature using Debye formula [34,47]. Two things from the figure should be noted; first, the frequency-dependent characteristic of the dielectric constant of water can clearly be observed. The real part of ε exhibits a falling trend and varies from about 74 to 29 within the band of interest. In the all-dielectric resonator design, the operating bandwidth of certain modes is usually narrow as the electrical size of the structure varies with frequency. Here the electrical size is defined as the ratio of the physical dimensions of the structure and operating wavelength. However, when the permittivity of the material also changes with frequency, this issue may be overcome. Based on this, the change in the dielectric constant of water provides an opportunity to design a water-based all-dielectric resonator with a broad mode bandwidth. Secondly, it can be seen that the imaginary part of the dielectric constant remains at a high level, indicating that the dielectric loss of water is quite high over the whole band.

Optical Materials EXPRESS

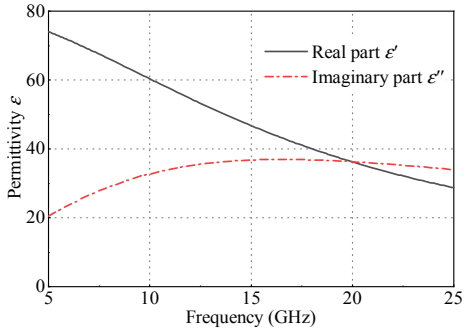

Fig. 2. Permittivity of water at 5–25 GHz obtained using Debye model.

The simulated absorption spectrum of the proposed cylindrical-water-resonator-based absorber is presented in Fig. 3(a) with a black line. The final optimized dimensions are given in Fig. 1. A high absorptivity can be observed over a wide operating band. The absorptivity of the proposed absorber is higher than 90% over the whole operating band from 5.58 to 24.21 GHz and the relative bandwidth can reach as high as 125%. In the operating band, four peak values can be found at 6.07, 8.10, 16.19, and 23.45 GHz, which has been marked as f_1 to f_4, respectively. The absorptivities at these frequencies are 99.15%, 96.95%, 98.89%, and 94.77%, respectively. The four absorption peaks indicate four resonances at these frequencies, in which the lower frequency points f_1 and f_2 correspond to the DR mode and the higher frequency points f_3 and f_4 correspond to the spoof SPP mode and grating mode, which will be analyzed in detail later. As the dielectric loss of water is quite high over the band of interest, another two water-based absorbers are also simulated for comparison. Case I is a water plate with the same height as that in the proposed absorber, and a metal plate is also placed on the back of the water plate. Case II is a water resonator without a metal back. In this case, the size of the water resonator and container is also the same as that in the proposed absorber. From Fig. 3(a), we can see that for Case I, the water plate can also absorb the incident wave, but the absorptivity is low, varying only between 0.3 and 0.45. This is primarily caused by the mismatch between the water plate and the air as the real part of water's dielectric constant is quite high compared to that of the air. The water resonator without the metal back used in Case II exhibits a different characteristic. An upward trend with frequency can be observed and the absorptivity varies from about 0.2 to 0.87. A local peak appears at 6.33 GHz, corresponding to the DR mode of the water resonator. With frequency increasing, the absorptivity increases and reaches the maximum at about 20.88 GHz. To investigate the reason of high absorptivity at this frequency, the power loss density in the resonator at 20.88 GHz are simulated and plotted in the inset of Fig. 1(a). With reference to the figure, one can see that the power loss mainly distributed at the top part of the resonator, indicating the grating mode is excited and good impedance matching between the resonator and air can be obtained, resulting in high absorptivity at certain frequency. As there is no metal back, the SPP mode cannot be excited for Case II. However, the absorptivity is relatively low over the whole band, and the highest value is only 0.869, which is not sufficient for microwave absorption. This comparison can prove that the high absorption is mainly caused by the strong resonance of the cylindrical water resonator.

To fully understand the operating principle of the proposed absorber, the simulated normalized input impedance calculated by the *S*-parameters is plotted in Fig. 3(b). It can be seen that at the four resonant points, f_1 to f_4, the imaginary part Z' is near-zero while the real part is near-unity, indicating that the absorber exhibits good impedance matching with air and the wave reflection at the absorber-air interface is quite low. The good impedance matching ensures that energy enters the absorber and is then totally absorbed because of the high dielectric loss of water.

Optical Materials EXPRESS

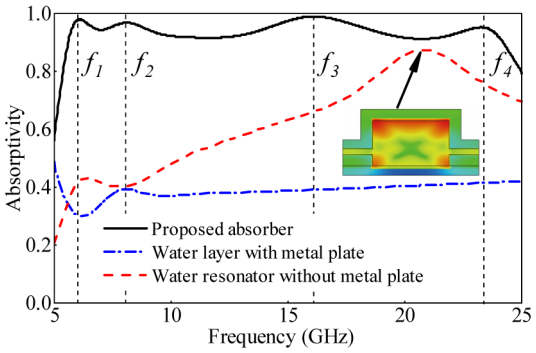

(a)

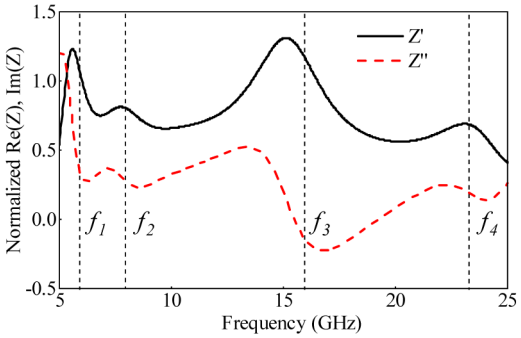

(b)

Fig. 3. (a) Simulated absorption spectra of proposed water-resonator-based absorber, metal-backed water plate, and cylindrical water resonator without metal back. The four absorption peaks of the proposed absorber have been marked as f_1, f_2, f_3, and f_4. Inset: Power loss density in the resonator for case II at 20.88 GHz. Blue represent the minimum power loss while red represents the maximum power loss. (b) Simulated input impedance of water-resonator-based absorber, with the four absorption peaks also marked.

The vector electric field (*E*-field), magnetic field (*H*-field) and the power-loss density in the resonator are also simulated to further investigate the working principle, and the results are presented in Fig. 4. In the simulation, the polarization of the incident wave is set as *x*-polarization. From the results in Figs. 4(a) and (b), a looped *E*-field distribution can be clearly found in the water resonator at f_1 = 6.07 GHz, while the *H*-field is a dipole-type, verifying that the DR mode, i.e. magnetic dipole mode, of the water resonator is excited. Comparing the field distribution at f_2 = 8.10 GHz with that at f_1, a quite similar behavior can be observed, indicating the similar resonant modes. This can be explained using the dielectric constant of water shown in Fig. 2. For a DR with fixed dimensions, the resonating frequency for a certain mode in the resonator can be considered as exhibiting a linear relationship with its electrical size, which can be determined using $\lambda/\sqrt{\varepsilon}$, where λ is the wavelength in free space. From Fig. 2, it can be seen that ε decreases with frequency, resulting in the electrical size of the resonator varying by a small amount over a wide band. This feature allows the DR mode to be maintained over a wide frequency band, manifested by multiple resonance points in the band, namely, f_1 and f_2. Thus, the changing dielectric constant of water can eliminate the effect caused by the changing electrical size of the resonator with frequency. In addition, with reference to the power loss density shown in Fig. 4(c) and (f), one can clearly see that the power loss occurs at every part of the water resonator, indicating the DR mode is excited and all of the power is absorbed by the water resonator.

Optical Materials EXPRESS

Next, the working principle at the frequency points f_3 is analyzed. As shown in Figs. 4(g) and (h), the incident wave is mainly confined between water resonator and metal plate. In this case, the array of water resonators acts as a grating and the spoof SPP mode that usually exists between the dielectric and metal can be excited. Usually, the SPP means the electromagnetic excitations that existing at the metal-dielectric interface. As the incident wave in this absorber is also confined at the interface of metal and dielectric, we use spoof SPP to describe this phenomenon and this is similar to the excited mode in [43], where the spoof SPP mode is excited using a hemispherical water resonator. Furthermore, with reference to Fig. 4(i), one can find the power loss is mainly distributed at bottom part of the water resonator, also indicating the spoof SPP mode is excited and most of the wave is confined at the surface of the metal and absorbed by the water resonator finally.

Finally, the working principle at the frequency point f_4 is analyzed. Observing the field distribution at the frequency, one can see that the E-field distribution is quite similar to that at f_3. However, the magnetic field is different. From the figure, it can be seen that the magnetic fields at the top part of the resonator and the gap between resonator and metal are all quite strong, indicating the hybrid mode, i.e. the combination of spoof SPP mode and grating mode, is excited. At same time, with reference to Fig. 4(l), one can see that the power loss is mainly distributed at the top part of the resonator, indicating the grating mode is dominate. Based on this, we can conclude that the high absorbance at this frequency is mainly caused by the grating mode. By combining the multiband of the dielectric mode, spoof SPP mode and grating mode, an ultra-broadband with high absorptivity can be obtained using the proposed absorber.

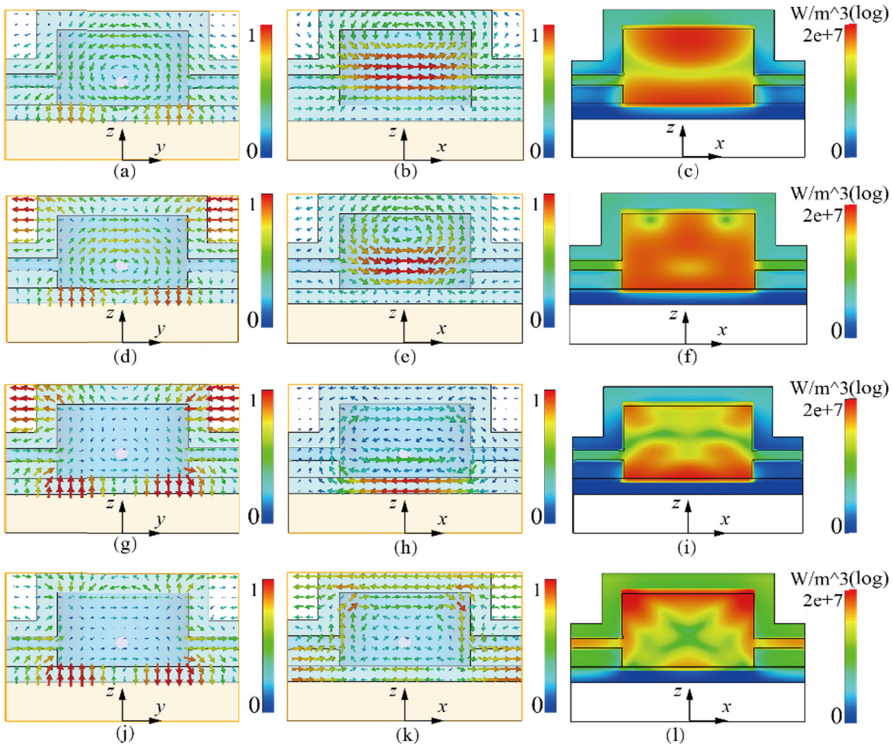

Fig. 4. Simulated vector field distribution in the absorber. (a, d, g, j) *E*-field in *xoz* plane for f_1, f_2, f_3, and f_4 of 6.07, 8.1, 16.19, and 23.45 GHz, respectively. (b, e, h, k) *H*-field in *yoz* plane for f_1, f_2, f_3, and f_4 of 6.07, 8.1, 16.19, and 23.45 GHz, respectively. (c, f, i, l) Power-loss density in *xoz* plane for f_1, f_2, f_3, and f_4 of 6.07, 8.1, 16.19, and 23.45 GHz, respectively.

Optical Materials EXPRESS

To verify the design, a prototype of the proposed absorber containing 15 × 15 unit cells shown in Fig. 1 is fabricated and measured. The total size of the absorber is 181 × 181 mm^2. Three-dimensional (3D) printing technology is used to manufacture the top resin cap and the PMMA bound to the resin cap, forming the whole container for the water resonator. A copper foil is attached to the back side of the PMMA, acting as the metal plate. Water is injected through the microchannel. The inset in Fig. 5 shows the prototype of the absorber. In order to investigate the absorption performance of the proposed absorber, the reflection coefficient of the absorber is measured using a vector network analyzer with two broadband horn antennas. A metal plate with the same size is also measured using the same method as the reference, and the reflectivity of the absorber is normalized to that of the metal plate. The simulated and measured results are presented in Fig. 5. A good agreement between the simulation and measurement can be observed from the results. In most of the band of interest, the absorptivity is higher than 90%. Some slight difference may be caused by imperfections in the fabrication process and the measurement error.

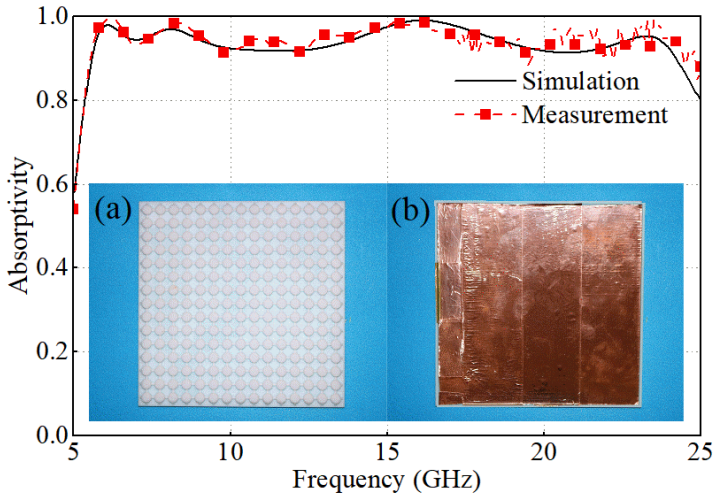

Fig. 5. Simulated and measured absorption spectra of the proposed absorber. Inset: Photo of absorber prototype with 15 × 15 elements. (a) Top view and (b) bottom view.

For fully evaluating the performance of the cylindrical-resonator-water-based absorber, the absorptivity under EM waves with different polarizations and angles of incidence are simulated, the results of which are presented in Fig. 6. Incident transverse electric (TE) and transverse magnetic (TM) modes are both considered and the angle of incidence varies from 0° to 45°. It can be seen from the figure that for the incident TM mode, the absorptivity remains higher than 90% over the whole operating frequency when the angles of incidence are below 30°. When the angles of incidence increase to 45°, the absorptivity is higher than 90% in most of the frequency band and higher than 85.5% over the rest of the band. For the case of the incident TE mode, as the angle of incidence increases, the absorptivity decreases in the lower frequency band while remaining higher than 90% in the higher frequency band. For angles of incidence below 45°, the absorptivity is higher than 77.6% over the whole operating frequency band.

It should be noted that there is a significant difference between the incident TE and TM modes in Fig. 6. This phenomenon can be understood with the help of the working principle. As mentioned above, in the lower frequency band, the DR mode, i.e., magnetic dipole mode, of the water resonator is excited. This DR mode is quite sensitive to the changing in intensity of the incident magnetic field. For the incident TE mode, when the angle of incidence increases, the magnetic field decreases, weakening the DR mode and thus decreasing the

Optical Materials EXPRESS

absorptivity significantly. However, compared with the DR mode, the spoof SPP mode and grating mode in the higher frequency band are not so sensitive to the magnetic field, and as the angle of incidence increases, the absorptivity will remain at a high level. This is consistent with the results presented in Fig. 6(a). For the incident TM mode, the change in magnetic field is small, and the electric field changes significantly with the increase in angle of incidence. As the excited modes are insensitive to the electric field, the absorptivity remains at high level over broad bandwidth. Based on the simulated results under different angles of incidence, the absorber performs well over a wide range of angles of incidence and broad operating band. Besides, it is noted that a water-based metamaterial absorber utilizing the DR mode and grating mode is proposed in [48] most recently. Different from the absorber proposed here, the DR mode of that absorber is dominated over very broad bandwidth, which may lead to significant decreasing in the absorptivity with incident angle increasing at certain frequencies. The absorber here can overcome this issue as the spoof SPPs mode and grating mode are insensitive to the incident angle as discussed above.

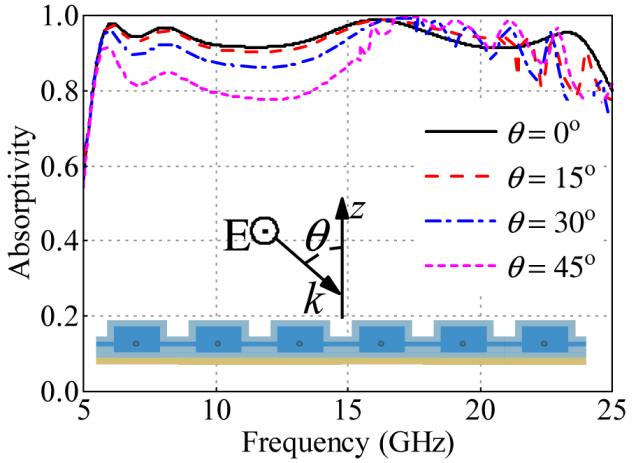

(a)

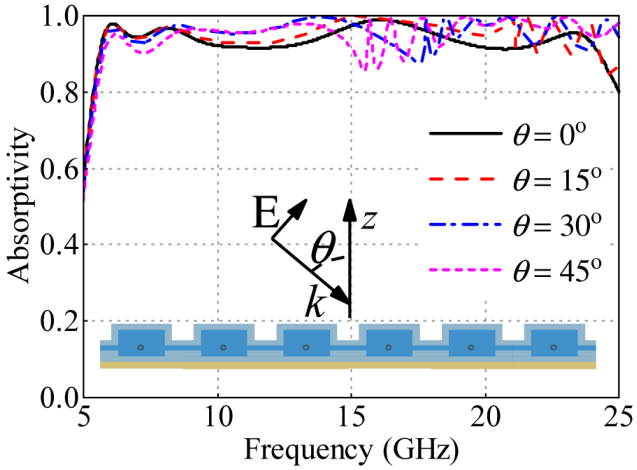

(b)

Fig. 6. Absorption spectra of the proposed water absorber for oblique-incidence waves with different angles of incidence and polarization states. (a) TE mode and (b) TM mode.

Optical Materials EXPRESS

As an absorber for transferring EM energy to thermal energy, the temperature of the water may change during the process of application. Meanwhile, water is a temperature-sensitive material whose dielectric constant and volume change with temperature. Thus, the absorptivity should be investigated under different temperatures and the temperature stability of the absorber should be discussed. The dielectric constant of the water under different temperatures can be predicted using the Debye formula [34,47], and the effect of the resin container and PMMA plate is not considered in the simulation. Figure 7 presents the absorption spectrum with the variation in temperature from 0° to 100°. It can be seen that the change in the absorptivity under different temperatures is quite small over the entire band of interest. When the temperature varies between 0° and 40°, the absorptivity remains higher than 90% from 5.58 to 24.21 GHz. When the temperature increases to 60°, the absorptivity decreases slightly in the lower frequency band but still remains higher than 87% over the operating band. When the temperature continues to increase, the absorptivity is higher than 78% over most parts of the operating band, except for some frequency points in the lower frequency band. Next, the thermal expansion of the water resonator is analyzed. When the temperature varies, the density of the water will change, leading to the volume of the resonator change accordingly. The volume changes of the water resonator can be calculated according to the experimental thermal-expansion data of the water [49]. As the water has smallest volume at 4 °C, here we consider the volume change between 4 °C and 100 °C, indicating the extreme case. In this case, the change of the volume of water can be calculated as about 4%. Considering the water absorber design here, if we fix the radius of the resonator, the resonator's height will change from 3.8 mm to 3.95 mm, which may have small impact on the performance of the absorber. However, it should be noted that the water container in this absorber is not sealed but open to the external via the microchannels. In the practice applications, a small external container connected to the microchannels can be included. When the volume of the water resonator increases with temperature increasing, the extra water will pass into the external container, making the size of the resonator unchanged. When the temperature decreases, this process is reversed. So, the thermal-expansion issue of the resonator can be addressed using this method. Based on the above analysis, we have reasons to believe that the proposed absorber weakly depends on the water temperature and can work steadily when the temperature changes significantly.

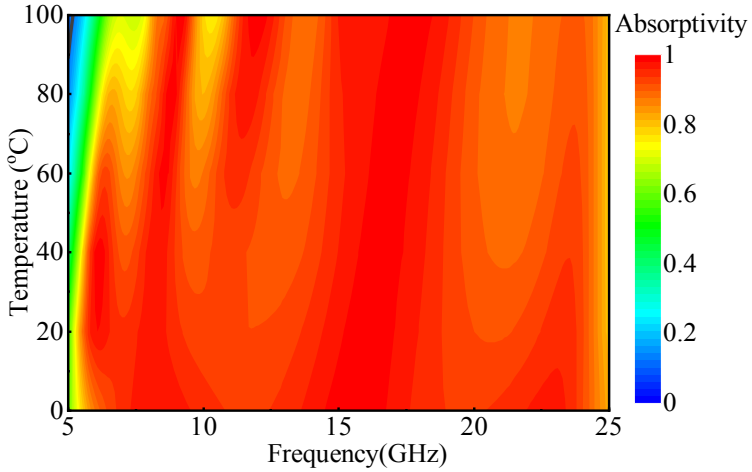

Fig. 7. Absorption spectrum of the absorber at different temperatures.

Recently, water has been widely used in the design of low-cost absorbers with high absorption for its high dielectric loss. This includes using the water plate as a dielectric substrate and water resonator with different shapes, such as droplets and cubes. To highlight

Optical Materials EXPRESS

the merits of the absorber presented here, a comparison with previous water-based absorbers is made and summarized in Table 1. It is clear from the table that the absorption bandwidth of the proposed absorber is the widest, with a value as high as 125%.

Table 1. Comparison between Proposed Absorber and Previous Water-based Absorber

Ref.	Absorber Type	Operating Band (GHz)	Relative Bandwidth (%)
[39]	Water resonator with droplet shape	8–18	76.9
[41]	Water plate with grid shape	8.1–22.9	95.5
[42]	Water as substrate	6.2–19	101.6
[43]	Water resonator with droplet shape	~17.2–40	78.9
[44]	Water resonator with rectangular shape	8.96–12.0	28.8
[45]	Water plate with hole array	12–29.6	84.6
[46]	Water resonator with droplet shape	7.5–15	66.7
[46]	Water cube	4.5–8	56
This work	Water resonator with cylindrical shape	5.58–24.1	125

4. Conclusions

In summary, a cylindrical-water-resonator-based absorber with an ultra-broad operating band is proposed in this paper. The DR mode of the water resonator is excited in the lower frequency band, whereas the spoof SPP mode and grating mode are excited in the higher frequency band. Benefiting from the advantage of the dielectric constant of water varying with frequency, the operating bandwidth of these two modes is quite wide. By optimizing the design, an ultra-broad operating band can be obtained with near-unity absorptivity. The measured results indicate that the absorptivity of the designed absorber is as high as 90% over almost the whole operating band from 5.55 to 24.1 GHz, with the relative bandwidth reaching 125%. The absorptivity under different polarized incident waves and angles of incidence are simulated for in-depth investigation. In addition, the thermal stability is investigated for evaluating the performance of the absorber. Further, through the microchannels, the water can be changed with other liquid, such as the mixture of water and ethyl alcohol and this provide the possibility to obtain reconfigurable absorber, which can be studied in future. The good performance of the absorber is promising for different applications such as low-cost anechoic chambers and stealth technology.